physica status solidi pss b

www.pss-b.com

Check for updates

Electron-Stimulated Aluminum Nitride Crystalline Phase Formation on the Sapphire Surface

Denis Milakhin, Timur Malin, Vladimir Mansurov, Yury Galitsyn, and Konstantin Zhuravlev*

The effect of a high-energy electron beam (11 keV) on the (0001) sapphire nitridation process is investigated. The high-energy electrons accelerate more than an order of magnitude the sapphire nitridation process. The effect is due to an increase of the Al and N atom concentrations on the sapphire surface caused by the electron-stimulated desorption of oxygen atoms and electron-stimulated decomposition of ammonia molecules.

1. Introduction

At present, direct-gap semiconductors with a band gap from 0.7 eV (InN) and 3.4 eV (GaN) to 6.2 eV (AlN) and their alloys attract considerable attention due to their wide practical application in creating light-emitting devices, UV photodetectors, and microwave and power transistors.[1–7] Great prospects are open for the application of graphene-like g-AlN and g-GaN layers in spintronics and electronics.[8,9]

To date, the most widely used substrate for the III-nitrides epitaxial growth is sapphire (α-Al_2O_3). Sapphire substrates are transparent in the UV and visible ranges, they are thermally stable and have good dielectric properties, which make them widely used in optoelectronics and microelectronics.[10]

The III-nitrides epitaxial growth process on sapphire substrates includes a number of special techniques typical for structures with a large mismatch between the crystal lattice parameters a and thermal expansion coefficients (CTE). These techniques ensure the parameters compatibility of sapphire lattice and subsequent layers ($a_{Sap} = 4.76$ Å, $CTE_{Sap} = 7.0 \times 10^{-6}$ K^{-1}, $a_{AlN/GaN} = 3.11$ Å/3.18 Å, $CTE_{AlN} = 4.2 \times 10^{-6}$ K^{-1}).[11,12] The sapphire nitridation process, as a mandatory initial stage in the III-nitrides growth, consists in exposing the heated sapphire substrate to a flux of active nitrogen.[2,13–20]

The sapphire nitridation process includes the following intermediate reactions and processes. Partial reduction of aluminum atoms from Al^{3+} to Al^{2+}, Al^{+} and the formation of AlO, Al_2O-oxides on the surface when the substrate is heated.[21] Dissociation of ammonia (NH_3) chemisorbed on sapphire surface to NH_2, NH-radicals. Recombination the part of ammonia radicals and the formation of nitrogen and hydrogen molecules. Nitrogen molecules, having strong triple covalent nonpolar bonds, not able to interact with aluminum. The interaction of the remaining ammonia radicals with the active reduced aluminum atoms with formation of crystalline aluminum nitride (AlN). These processes were studied in detail and described elsewhere.[2,4,19,22–24]

The method of reflection high-energy electron diffraction (RHEED) is widely used to register and study the nitridation process.[25,26] In this method, the main tool for studying the surface is elastically scattered high-energy electrons. Despite a large number of papers devoted to the study of high-energy electrons influence on solid properties, it is believed, that these electrons do not have a significant impact on the processes occurring on the grown structure surface.[27,28]

In this paper, we show that the high-energy electrons used in the RHEED technique affect the sapphire nitridation process. The mechanisms of the influence are discussed.

2. Experimental Section

Investigations were carried out in a Riber CBE-32P MBE machine. As nitrogen source, the ammonia with special purity 99.999% was used. The experiments were carried out on 2" (0001)-oriented sapphire substrates. On the underside of the substrate, a 0.4 μm thick layer of molybdenum was deposited to absorb thermal radiation from the heater, since sapphire is insensitive to infrared radiation. Since sapphire is a good dielectric with the bandgap 9.5 eV a charge accumulates on the sapphire surface during electron irradiation that distorts and smears the diffraction pattern. To reduce the effect of charging, the sapphire surface was covered with a 0.15 μm thick layer of molybdenum, except research region with a diameter of 5 mm. For the preliminary cleaning, substrates were annealed in the loading chamber at the temperature of 1170 K in the residual atmosphere of (2–5) × 10^{-8} Torr. The substrate temperature was registered using an Ircon infrared-type pyrometer.

D. S. Milakhin, T. V. Malin, Dr. V. G. Mansurov, Dr. Yu. G. Galitsyn, Dr. K. S. Zhuravlev
Rzhanov Institute of Semiconductor Physics
Siberian Branch of the Russian Academy of Sciences
13, Lavrentiev Avenue, Novosibirsk 630090, Russia
E-mail: dmilakhin@isp.nsc.ru

Dr. K. S. Zhuravlev
Novosibirsk State University
Pirogov str. 1, Novosibirsk 630090, Russia

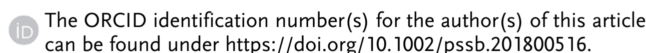
The ORCID identification number(s) for the author(s) of this article can be found under https://doi.org/10.1002/pssb.201800516.

DOI: 10.1002/pssb.201800516

© 2019 WILEY-VCH Verlag GmbH & Co. KGaA, Weinheim

The electron gun model CER 606 was used as a source of high-energy electrons in the RHEED setup. The cathode material is tungsten. According to published data under standard conditions (modulator voltage 11 kV, filament current 1.6 A) the electron gun provides an emission current of about 100 μA. According to the Richardson–Deshman formula, the emission current density depends exponentially on the cathode temperature. The cathode temperature was evaluated using the Stefan-Boltzmann law. It was assumed that the filament current is expended mainly on cathode heating and dissipated in the thermal radiation form. To control the emission current magnitude, the integrated emission intensity I of a luminescent screen was measured by directing the high-energy electrons to the screen. The luminescent screen was made of polycrystalline gadolinium oxysulfide doped with ytterbium (Gd_2O_2S:Yb), having a high cathodoluminescence efficiency. The luminescent screen intensity grew linearly, proportionally to the increase in the emission current in the filament current range of 1.6–1.8 A. In the experiments the luminescent screen intensity was 145 arb. unit for 1.6 A, 195 arb. unit for 1.7 A and 245 arb. unit for 1.8 A, respectively.

The sapphire surface was exposed in the ammonia flux of 25 sccm at the substrate temperature of 1170 K. An electron beam fell on the sapphire surface at an angle of 1–3°. The diffraction patterns (DP) were recorded by the kSA 400 analytical analysis system equipped with a high-resolution CCD camera with high sensitivity optics, specially developed for RHEED technique.

3. Results

3.1. Nitridation Process Under the Action of High-Energy Electrons

The formation of the crystalline AlN on a heated sapphire substrate under the ammonia influence is manifested in the change of DP from the substrate surface. The inset to **Figure 1** shows two diffraction patterns of clean sapphire (left) and nitrided sapphire (right). After a 10-min exposure to the 25 sccm ammonia flux, the diffraction pattern of the sapphire surface changes. The intensity of the sapphire 01, 02, and 03 reflexes decreases. Near the sapphire 00 and 03 reflexes, located near the symmetric azimuth [11–20], new 00 and 01 reflexes appear, which are located close to the symmetric azimuth [10–10]. The space between the newly formed 00 and 01 reflexes and their position relative to the sapphire reflexes corresponds to the crystalline AlN.[29,30]

The dependences of the 01 AlN reflex intensity a on the time at continuous irradiation with various fluxes of high-energy electrons are shown in Figure 1. All curves were normalized to the maximum reflex intensity. The intensities of the 01 AlN reflex increase with time and then saturate. The intensity growth is associated with an increase of the formed AlN nuclei number.[19,20] According to the following kinetic Equation (1), the crystalline AlN formation under certain probability k_2 is limited by the concentration of active partially reduction aluminum since the ammonia flux was fixed.[19]

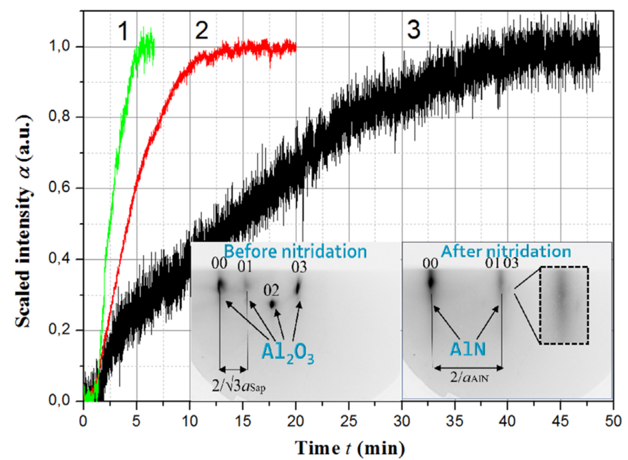

Figure 1. The kinetic curves of the 01 AlN reflex intensity under continuous different e-beam fluxes ($I = 145$ arb. unit for curve 3, 195 arb. unit for curve 2 and 245 arb. unit for curve 1). The inset to **Figure 1** shows the diffraction pattern of clean Al_2O_3 before nitridation (left) and the diffraction pattern of nitrided Al_2O_3 with the reflexes from AlN formed (right).

$$\frac{d[AlN]}{dt} = k_2 \cdot [NH_2] \cdot [AlO] \quad (1)$$

During nitridation process the concentration of active aluminum atoms decreases, slowing down the AlN formation kinetics. Over time, the concentration of active aluminum decreases so much so the 01 AlN reflex intensity does not change, and we observe a saturation region on the kinetic curves.

The average growth rate v of the intensity was determined as the ratio of the intensity change a to time t at saturation point ($\Delta a/\Delta t$). The average rate of the nitridation process increases in 7.5 times with the electron flux growth in 1.7 times.

Figure 2 demonstrates the kinetics curves of the 01 AlN reflex intensity under the electron beam pulsed action at fixed fluxes of high-energy electrons being $I = 195$ arb. unit. The pulse duration was $\tau = 60$ s for the duty cycle $S = 2$ and $\tau = 15$ seconds for $S = 20$. For comparison, the nitridation kinetic curve, measured with continuous action of the electron beam, is also shown. The kinetic curves character depends on the duty cycle and the duration of the surface irradiation by an electron beam.

Having determined the average nitridation process rate, we estimated that the AlN nitridation kinetics at duty cycle $S = 2$ and the pulse duration 60 s is 5 times higher than the nitridation kinetics at duty cycle $S = 20$ with the 4 times lower pulse duration. With continuous electrons irradiation of the sapphire surface, the kinetics of AlN crystalline phase formation was fastest, and it exceeded the nitridation kinetics at duty cycle $S = 20$ seven times. Thus, the longer the process of sapphire surface irradiation with electrons in the ammonia atmosphere, the faster the AlN crystalline phase formed.

The curves 2 and 3 show that the electron beam affects the nitridation process only at 50 and 5%, respectively, from the total sapphire surface exposure time in the ammonia atmosphere. Knowing the average nitridation rates of electron continuous and pulsed irradiation, the average rate of nitridation process

© 2019 WILEY-VCH Verlag GmbH & Co. KGaA, Weinheim

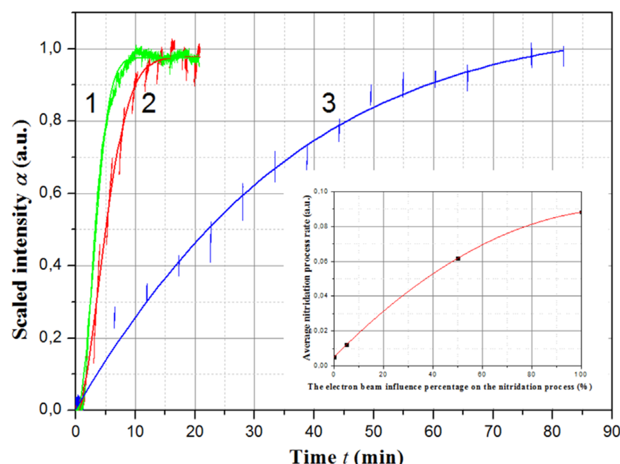

Figure 2. 01 AlN reflex intensities dependence on the nitridation time at the continuous (curve 1) and pulsed actions of electrons: pulse duration $\tau = 60$ s. and duty cycle $S = 2$ (curve 2), $\tau = 15$ s. and $S = 20$ (curve 3). The inset to **Figure 2** shows the dependence of the average nitridation process rate from the electron beam influence percentage on the nitridation process.

without high-energy electrons action in the inset to Figure 2 (intersection point of the approximation curve with the y-axis) was estimated. As it turned out, it is almost 17 times slower than it was obtained from the RHEED data, under the continuous electrons irradiation. Curiously enough that even 15-s irradiation by electrons every other 5 min accelerates the nitridation process in 2.5 times. Thus, there is a significant electrons influence on the crystalline AlN formation rate.

3.2. Mechanisms of Electron Beam Influence on Sapphire Nitridation

All effects that occur when high-energy electrons interact with atoms and molecules in both the surface and bulk of the substrate are the results of electronic subsystem excitation processes that can lead to a material heating, electron-stimulated decomposition, and desorption.[31] During the sapphire surface irradiation by high-energy electrons, the crystal lattice gets additional energy, causing a temperature increase in the beam effect region. Heat energy is transferred to the reacting particles, accelerating the nitridation process. To estimate the degree of sapphire heating, we used the Equation (2) describing the temperature change ΔT in time t on the sapphire surface irradiated by the electron beam[32]:

$$\Delta T = \frac{E_0}{Kd} \cdot \frac{arctan\left(2\sqrt{\frac{kt}{d^2}}\right)}{\pi^{\frac{3}{2}}} \qquad (2)$$

Here $k = K/\rho \times C$, k is the thermal diffusivity, ρ is the sapphire density equal to 3980 kg m^{-3}, K is the sapphire thermal conductivity equal to 9.1 W m^{-1} K^{-1}, C is the thermal capacitance equal to 1214.9 J kg^{-1} K^{-1} (these table values correspond to the sapphire substrate temperature 1100 K); E_0 is the beam energy deposited per second with the emission current $I_e \sim 100$ μA and the voltage at the control electrode $U = 11$ kV, d is the width parameter for the Gaussian beam profile, t is the exposure time of the electron beam $t \rightarrow \infty$.

Equation (2) describes the temperature change ΔT, taking into account the transfer of all electrons energy to the crystal. According Monte Carlo simulation of the high-energy electron beam interaction with sapphire substrate, the condition of highest energy transfer can be accomplished only at the angle of incidence of 90° (Figure S1, Supporting Information). In this case, about ≈96% electrons are in elastically scattered into the substrate and heat the sample to ≈17.2 K during thermalization process. Considering that in RHEED method an electron beam falls on the crystal at a glancing angle of ≈3° (Figure S2, Supporting Information), about 86% of incident electrons are reflected from sapphire with minor energy losses, and only ≈14% of incident electrons are inelastically scattered and heat the substrate to 2.4 K. The electron beam pulsed action reduces the substrate heating. By

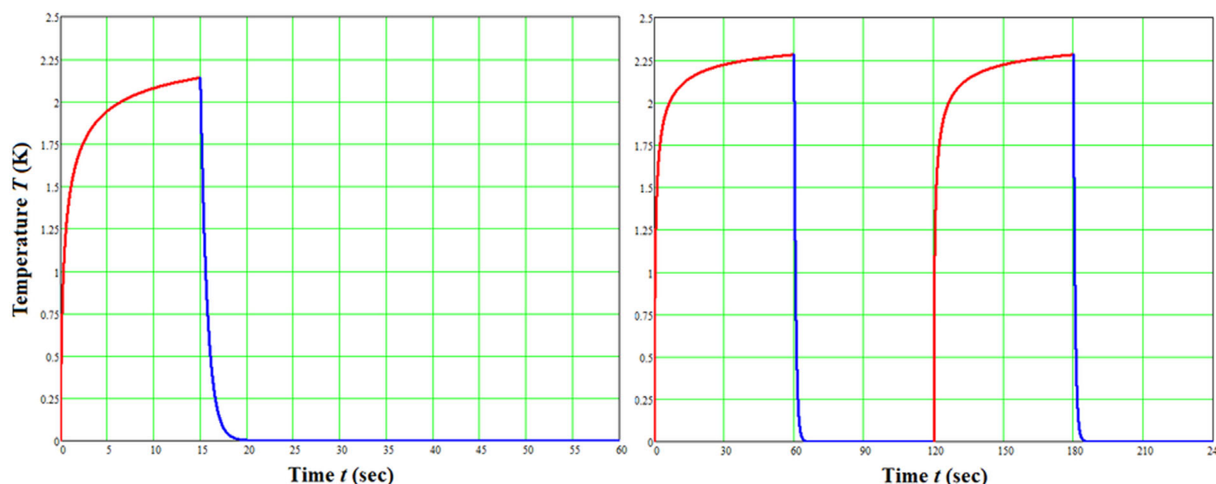

Figure 3. Graph of the change in the substrate temperature in the region of the high-energy electron beam action in time t with the duty cycle $S = 20$ (left) (for illustrative purpose the dependence in the first 60 s is shown) and $S = 2$ (right). The process of body cooling was expressed through Newton's law of cooling.

© 2019 WILEY-VCH Verlag GmbH & Co. KGaA, Weinheim

first 15 s the substrate temperature increases only by 2.1 K and by the next 45 s the temperature varies less than 1 K (**Figure 3**). Between pulses the temperature has time to equalize across the entire sample through Newton's law of cooling. As a result, the average temperature of the nitrided substrate rises less than 1 K. Such temperature growth has an insignificant effect on the nitridation process probability.[30]

Electrons are supposed to affect the concentration of reacting particles. During irradiation the primary inelastically scattered electrons initiate an avalanche process of the secondary electrons generation with a wide energy ranges. It is well known that for many insulators the yield of secondary electrons is greater than the incident electron flux.[33] The backscattered electrons perform several collisions with lattice losing ≈tens of eV. As a result of a cascade of inelastic scattering processes, electrons are able to generate electron-hole pairs.

The AlO-oxides reacting particles formation on the surface is described by the following equation,[30]

$$Al_2O_3 \rightarrow 2AlO + \tfrac{1}{2}O_2 \quad (3)$$

The reduced state of aluminum in the form of AlO particles plays a significant role in nitridation process. Consider the processes involving generated holes, leading to the desorption of oxygen and to an increase of concentration the reduced aluminum. On the surface, the capture of holes by oxygen atoms leads to the formation of weakly bound oxygen O^- (Equation (4)), which in turn can pass into the O^{Chem} chemisorbed state (Equation (5)). The recombination of O^{Chem} leads to the desorption of oxygen in the form of an O_2 molecule (Equation (6)) followed by surface oxygen vacancies formation. In this case, the particles emission from the surface is called electron-stimulated desorption (ESD).[34] In parallel to oxygen ESD process high-energy electrons can initiate the ammonia decomposition process. The presence of surface oxygen vacancies sustains to electron-stimulated dissociation of NH_3 molecule (binding energy N-H ≈4 eV) on the surface.[35] Atomic nitrogen, which is the final product of this dissociation process, chemically interact with the reduced aluminum to AlN formation.

$$O^{2-} + \text{hole} \leftrightarrow O^- \quad (4)$$

$$O^- \leftrightarrow O^{Chem} \quad (5)$$

$$O^{Chem} + O^{Chem} \rightarrow O_2\uparrow \quad (6)$$

Thus, the acceleration of the AlN crystalline phase formation under the influence of a high-energy electron beam up to 17 times is mainly due to summarizing the electron-stimulated desorption of oxygen and electron-stimulated dissociation processes, which increase the concentration of active aluminum and nitrogen. The heat energy transferred from ≈14% inelastically scattered electrons is distributed over the crystal volume and is not capable of significantly affecting the crystalline AlN formation.

4. Conclusion

Investigations have shown that, when the electron beam influence is excluded, the AlN crystalline phase formation process is much slower and can differ by more than an order of magnitude from the nitridation process under an intense continuous action of the beam. The acceleration of the AlN crystalline phase formation is caused by electron-stimulated oxygen desorption and electron-stimulated dissociation of ammonia molecules, nor than local heating, as might be expected primarily. Thus, by using the methods of studying a crystalline structure by electrons (Auger electron spectroscopy, reflection high- and low-energy electron diffraction, electron energy loss spectroscopy, etc.), its influence on surface processes can be taken into account and minimized.

Supporting Information

Supporting Information is available from the Wiley Online Library or from the author.

Acknowledgement

We are grateful to RFBR (under grants no. 17-02-00947 and 18-52-00008).

Conflict of Interest

The authors declare no conflict of interest.

Keywords

III-nitrides, ammonia-MBE, electron-stimulated processes, nitridation, reflection high-energy electron diffraction (RHEED)

Received: September 28, 2018
Revised: December 15, 2018
Published online:

[1] S. Strite, H. Morkoc, *J. Vac. Sci. Technol. B* **1992**, *10*, 1237.
[2] K. Uchida, A. Watanabe, F. Yano, M. Kouguchi, T. Tanaka, S. Minagawa, *J. Appl. Phys.* **1996**, *79*, 3487.
[3] S. Nakamura, T. Mukai, M. Senoh, *Jpn. J. Appl. Phys., Part 2* **1991**, *30*, L1708.
[4] Y. Cho, Y. Kim, E. R. Weber, S. Ruvimov, Z. Liliental-Weber, *J. Appl. Phys.* **1999**, *85*, 7909.
[5] Y. Saito, T. Akiyama, K. Nakamura, T. Ito, *J. Cryst. Growth* **2013**, *362*, 29.
[6] A. Alekseev, D. M. Krasovitsky, S. I. Petrov, V. P. Chaly, *Semiconductors* **2012**, *46*, 11.
[7] I.-S. Yu, C.-P. Chang, C.-P. Yang, C.-T. Lin, Y.-R. Ma, C.-C. Chen, *Nanoscale Res. Lett.* **2014**, *9*, 682.
[8] C. L. Freeman, F. Claeyssens, N. L. Allan, J. H. Harding, *Phys. Rev. Lett.* **2006**, *96*, 066102.
[9] V. Mansurov, T. Malin, Yu. Galitsyn, K. Zhuravlev, *J. Cryst. Growth* **2015**, *428*, 93.
[10] H. Ishikawa, K. Yamamoto, T. Egawa, T. Soga, T. Jimbo, M. Umeno, *J. Cryst. Growth* **1998**, *189/190*, 178.

© 2019 WILEY-VCH Verlag GmbH & Co. KGaA, Weinheim

[11] T. Yamaguchi, T. Araki, Y. Saito, K. Kano, H. Kanazawa, Y. Nanishi, N. Teraguchi, A. Suzuki, *J. Cryst. Growth* **2002**, *237-239*, 993.
[12] K. Masu, Y. Nakamura, T. Yamazaki, T. Shibata, M. Takahashi, K. Tsubouchi, *Jpn. J. Appl. Phys*. **1995**, *34*, L760.
[13] Ch. Heinlein, J. Grepstad, T. Berge, H. Riechert, *Appl. Phys. Lett* **1997**, *71*, 341.
[14] A. Georgakilas, S. Mikroulis, V. Cimalla, M. Zervos, A. Kostopoulos, Ph. Komninou, Th. Kehagias, Th. Karakostas, *Phys. Status Solidi A* **2001**, *188*, 567.
[15] F. Dwikusuma, T. F. Kuech, *J. Appl. Phys*. **2003**, *94*, 5656.
[16] B. Agnarsson, M. Göthelid, S. Olafsson, H. P. Gislason, U. O. Karlsson, *J. Appl. Phys*. **2007**, *101*, 013519.
[17] N. Grandjean, J. Massies, M. Leroux, *Appl. Phys. Lett*. **1996**, *69*.
[18] M. Yeadon, M. T. Marshall, F. Hamdani, S. Pekin, H. Morkoc, J. Murray Gibson, *J. Appl. Phys*. **1998**, *83*, 2847.
[19] T. V. Malin, V. G. Mansurov, Y. G. Galitsyn, K. S. Zhuravlev, *Phys. Status Solidi C* **2014**, *11*, 613.
[20] T. V. Malin, V. G. Mansurov, Y. G. Galitsyn, K. S. Zhuravlev, *Phys. Status Solidi C* **2015**, *12*, 443.
[21] T. M. French, G. A. Somorjai, *J. Phys. Chem*. **1970**, *74*, 2489.
[22] D. S. Milakhin, T. V. Malin, V. G. Mansurov, Yu. G. Galitsyn, K. S. Zhuravlev, *Semiconductors* **2015**, *49*, 905.
[23] E. Fattal, M. Radeke, G. Reynolds, E. A. Carter, *J. Phys. Chem. B* **1997**, *101*, 8658.
[24] C. A. Pignedoli, R. Di Felice, C. M. Bertoni, *Phys. Rev. B* **2001**, *64*, 113301.
[25] P. J. Dobson, B. A. Joyce, J. H. Neave, J. Zhang, *J. Cryst. Growth* **1987**, *81*, 1.
[26] J. Schörmann, S. Potthast, D. J. As, K. Lischka, *Appl. Phys. Lett*. **2007**, *90*, 041918.
[27] C. Bater, J. H. Campbell, J. H. Craig, Jr., *Surf. Interface Anal*. **1998**, *26*, 97.
[28] C. J. Lobo, A. Martin, M. R. Phillips, M. Toth, *Nanotechnology* **2012**, *23*, 375302.
[29] T. Malin, D. Milakhin, V. Mansurov, Yu. Galitsyn, A. S. Kozhuhov, V. V. Ratnikov, A. N. Smirnov, V. Yu. Davydov, K. S. Zhuravlev, *Semiconductors* **2018**, *52*, 789.
[30] D. S. Milakhin, T. V. Malin, V. G. Mansurov, Y. G. Galitsyn, K. S. Zhuravlev, *J. Therm. Anal. Calorim*. **2018**, *133*, 1099.
[31] C. G. Pantano, A. S. D'Souza, A. M Then, In *Methods of surface characterization* (Eds: Alvin W. Czanderna, Theodore E. Madey, and Cedric J. Powell), Vol. *5*, Kluwer Academic Publishers, New York, Boston, Dordrecht, London, Moscow **2002**, Ch. 2.
[32] R. Gossink, H. Van Doveren, J. A. T. Verhoeven, *J. Non-Cryst. Solids* **1980**, *37*, 111.
[33] A. J. Decker, *Solid State Phys*. **1958**, *6*, 251.
[34] T E Madey, *Surf. Sci*. **1994**, *299/300*, 824.
[35] U. Diebold, T. E. Madey, *J. Vac. Sci. Technol. A* **1992**, *10*, 2327.

© 2019 WILEY-VCH Verlag GmbH & Co. KGaA, Weinheim